Supplementary Information (SI) for Chemical Science.
This journal is © The Royal Society of Chemistry 2025

Supporting Information

Amino-Induced Cleavage of Electron-Communicating S-Bridge to Unlock Mixed-Valence Copper for Potent Oxidase-like Catalysis and Selective Sensing

Bojin Li,[a] Nannan Xia,[b] Chaofeng Huang,*[c] Xun Hu,*[a] Fei He*[a]

[a] School of Material Science and Engineering, University of Jinan, Jinan 250024, China

[b] State Key Laboratory of Green Papermaking and Resource Recycling, Key Laboratory of Pulp & Paper Science and Technology of Shandong Province/Ministry of Education, Qilu University of Technology (Shandong Academy of Sciences), Jinan 250353, China

[c] School of Chemistry and Chemical Engineering/State Key Laboratory Incubation Base for Green Processing of Chemical Engineering, Shihezi University, Shihezi 832000, China

(*) E-mail: cf.huang@shzu.edu.cn; xun.hu@outlook.com; mse_hef@ujn.edu.cn

Experimental Section

Chemicals: 2-amino-5-mercapto-1,3,4-thiadiazole (AMTD, 97%) and 2-mercapto-1,3,4-thiadiazol (MTD, 99.88%) were purchased from Bidepharm. L-Ascorbic acid (AA, 99.7%) and L-Dehydroascorbic acid (DHAA) were purchased from Sinopharm Chemical Reagent Co., Ltd (Shanghai, China) and Macklin, respectively. $CuSO_4$ was purchased from DAMAO. Ultrapure water was obtained using a Taiping-M pure water purification system (China). All solvents were of analytical grade and used without further purification.

Preparation of Cu-AMTD: To a solution of 2-amino-5-mercapto-1,3,4-thiadiazole (AMTD, 2.0 g) in DMF (200 mL), an aqueous solution of $CuSO_4$ (1.17 g in 250 mL H_2O) was added. After stirring at room temperature for 24 h, the mixture was centrifuged. The collected solid was washed sequentially with NMP, H_2O, ethanol, and diethyl ether, then dried under vacuum at 70 °C to afford Cu-AMTD (0.31 g).

Preparation of Cu-MTD: To a stirred solution of 2-mercapto-1,3,4-thiadiazole (MTD, 2.0 g) in dimethylformamide (DMF, 200 mL) was added an aqueous solution of copper(II) sulfate ($CuSO_4$, 1.17 g in 250 mL H_2O). The mixture was stirred at ambient temperature for 24 h. The resulting solid was

isolated by centrifugation, washed sequentially with NMP, deionized water, ethanol, and diethyl ether, and subsequently dried under vacuum at 70 °C to yield Cu-MTD as a solid (0.32 g).

Evaluation of the catalytic kinetics: Quantitative assessment of the catalytic activity of nanozyme was performed using Michaelis-Menten kinetics. The kinetic parameters, namely the Michaelis constant (K_m), maximum velocity (V_{max}), catalytic rate constant (K_{cat}), and catalytic efficiency (K_{cat}/K_m), were determined by fitting the initial rate based on the Michaelis-Menten equation:[1]

$$V = V_{max} \times [S]/(K_m + [S])$$

where V and V_{max} represented the initial and maximal reaction velocities, respectively. [S] was the concentration of substrate. K_{cat} was obtained according to the equation: $K_{cat} = V_{max}/[E]$, where [E] represented the concentration of nanozyme.

10μL of nanozyme (1 mg mL^{-1}) and 1.5~20 μL of AA (1 mM) were added to 500 μL of PBS buffer solution (pH=7.2). The characteristic absorption peak at 266 nm attributable to AA was monitored over time.

Evaluation of electron transfer capability of nanozyme: 1.0 mg of the nanozyme powder was mixed with acetonitrile (980 μL) and a 20 μL TCNQ stock solution (5 mM) in a reaction vial. The resulting suspension was heated to 80 °C with magnetic stirring for 20 min. Following centrifugation, the supernatant was carefully monitored for UV-vis spectroscopic analysis.

Electrochemical measurement: Electrochemical measurements were performed using a CHI760E electrochemical workstation in a standard three-electrode system. A nanozyme-modified rotating disk glassy carbon electrode (RDE) served as the working electrode, with a graphite rod and a saturated calomel electrode (SCE) as the counter and reference electrodes, respectively. The working electrode was prepared by casting 10 μL of a nanozyme dispersion in ethanol (5 mg mL^{-1}) onto the pre-polished glassy carbon surface (5 mm diameter). After air-drying at room temperature, 10 μL of Nafion solution (0.05 wt %) was applied as a protective layer. Phosphate buffered solution (PBS, pH 7.2) was used as the electrolyte for both oxygen reduction reaction (ORR) and ascorbic acid (AA) oxidation studies. For AA oxidation experiments, the PBS electrolyte (pH 7.2) was either Ar- or O_2-saturated and contained 28.4 mM AA.

According to the linear sweep voltammetry (LSV) of RRDE measurement at 1600 rpm, the H_2O_2 yields and the electron transfer number (n) were calculated based on the following equation:[2]

$$H_2O_2\ (\%) = 200 \times \frac{I_R/N_0}{(I_R/N_0) + I_D}$$

$$n = 4 \times \frac{I_D}{(I_R/N_0) + I_D}$$

where I_D and I_R represented the disk current and ring current, respectively. The N_0 represented the current collection efficiency of RRDE, which was determined to be 0.29.

Detection of tris(2-carboxyethyl)phosphine (TCEP): The reaction was initiated by mixing 10 μL of TCEP (218.17 ppm), 10 μL of AA (10 mM), 10 μL of nanozyme (1 mg mL^{-1}), and 470 μL of PBS (pH 8.0) at room temperature. After incubation for 3 minutes, the mixture was analyzed via UV-vis spectroscopy.

Determination of Linear relationship between absorbance and TCEP concentration: At room temperature, 10 μL of TCEP (43.63~305.43 ppm), 10 μL of AA (10 mM), 10 μL of nanozyme (1 mg mL^{-1}), and 470 μL of PBS (pH 8.0) were combined. The mixture was incubated for 3 minutes before analysis using UV-vis spectroscopy to monitor the characteristic absorption peak at 266 nm.

Selectivity of Cu-AMDT for detecting TCEP in the presence of interfering compounds: To assess the selectivity of Cu-AMDT for TCEP, control experiments were conducted using 5 ppm potential interfering compounds (KNO_3, KCl, Na_2SO_4, glucose, triethyl phosphate, or tripropyl phosphate) instead of TCEP. The reaction mixtures were incubated for 3 minutes, and then monitored using UV-vis spectroscopy.

Determination of reduction capability of TCEP for the oxidation product of AA (i.e., DHAA): 10 μL of TCEP (218.17 ppm), 10 μL of DHAA (10 mM), and 480 μL of PBS solution (pH=8.0) were mixed and allowed to react for 2 minutes. The resulting mixture was subsequently analyzed by UV-vis spectroscopy.

Characterizations

X-ray photoelectron spectroscopy (XPS) spectra were conducted on a Thermo Scientific K-Alpha (USA) with hν 1486.6 eV. Electron spin resonance (ESR) spectra were collected using Bruker EMXplus-6/1 (Germany). Inductively coupled plasma optical emission spectrometry (ICP-OES) measurement was performed using Agilent 5110 (USA). Transmission electron microscopy (TEM) image was collected on a JEM-2100 Plus microscope (JEOL, Japan). Scanning electron microscopy (SEM) images

were recorded on a ZEISS Sigma 360 (Germany) scanning electron microscope at an acceleration voltage of 3 kV. Energy dispersive X-ray spectroscopy was obtained on an OXFORD XPLORE30 at an acceleration voltage of 10 kV. UV-vis absorption spectroscopy was measured on a UV-2600i UV-vis spectrophotometer (Japan). X-ray absorption fine structure (XAFS) spectroscopy was carried out using the RapidXAFS 2M (Anhui Absorption Spectroscopy Analysis Instrument Co., Ltd.) by transmission (or fluorescence) mode at 20 kV and 20 mA, and the Si (553) spherically bent crystal analyzer with a radius of curvature of 500 mm was used for Cu.

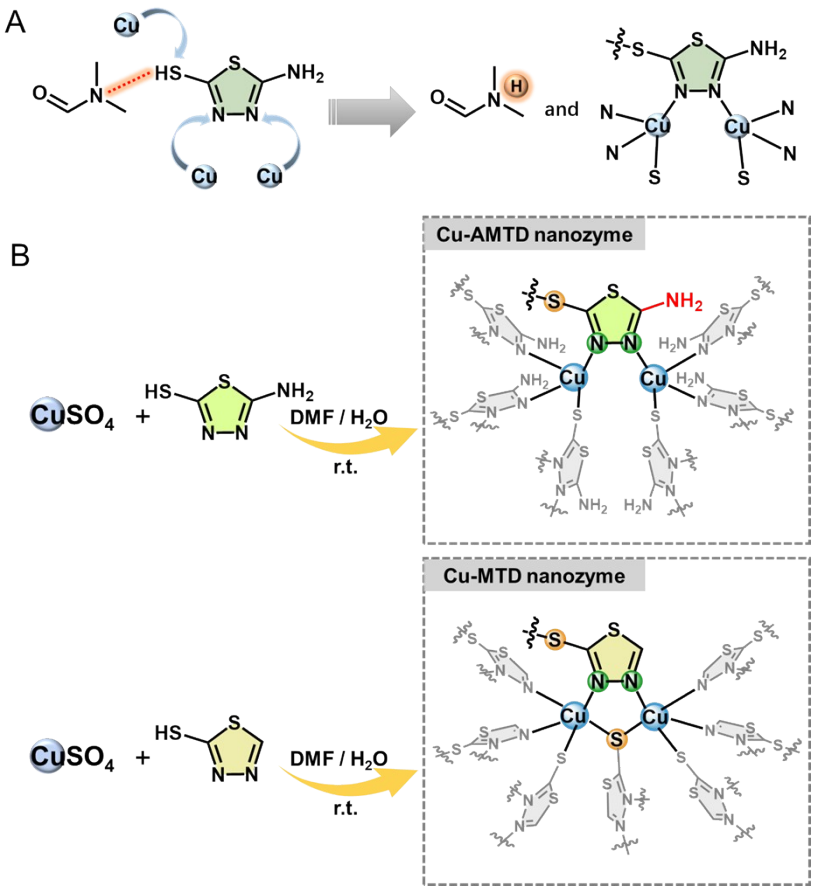

Scheme S1 (A) Typical coordination mechanism between Cu and AMTD; (B) Synthetic routes for preparing Cu-AMTD and Cu-MTD.

The S atom in the thiadiazole heterocycle often presented poor coordination capability for Cu[3,4]. However, in presence of N, N-dimethylformamide (as an alkaline reaction environment for preparing Cu-MTD and Cu-AMTD), the -SH group was easy to coordinate with Cu to form Cu-S bond, accompanied by the loss of a hydrogen atom. Therefore, the coordination may mainly occur between Cu and-SH as well as two neighboring heterocyclic N atoms.

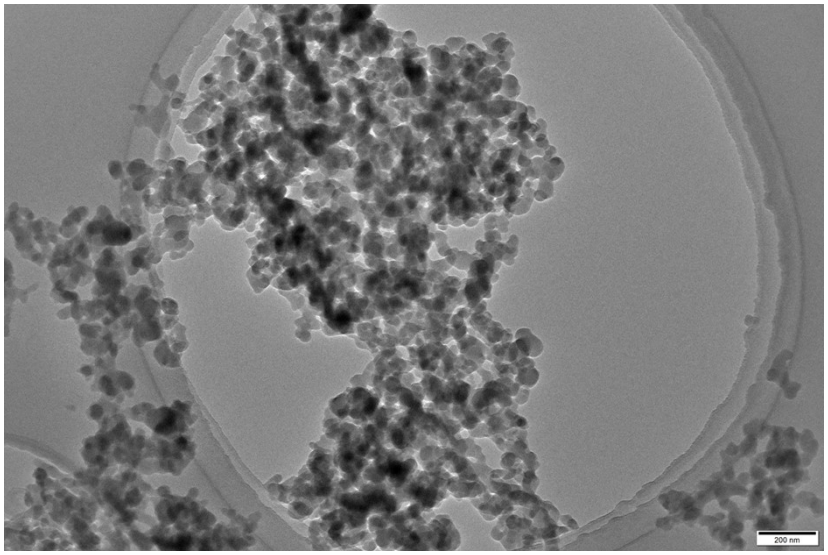

Figure S1 TEM image of Cu-MTD.

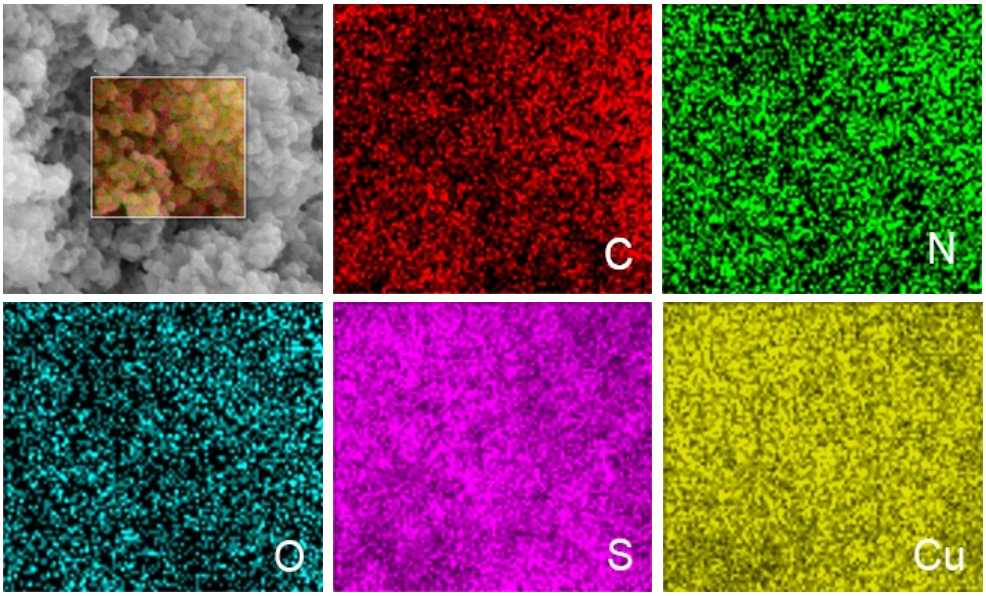

Figure S2 EDS mapping of Cu-MTD.

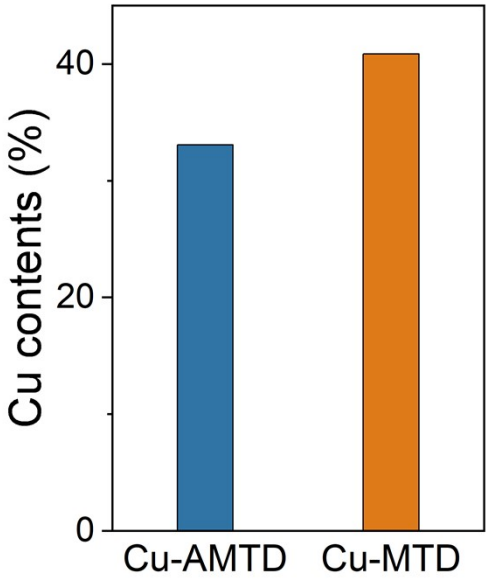

Figure S3 Cu contents (ICP-OES) of Cu-AMTD and Cu-MTD.

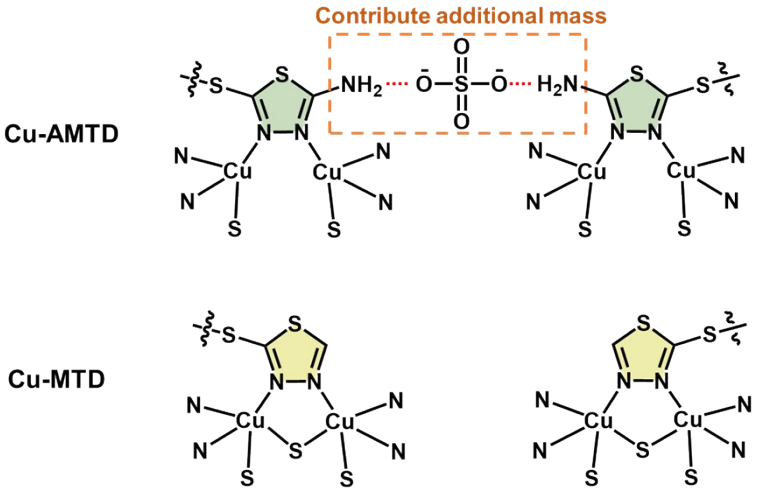

Figure S4 Understanding how contribution from the incorporated SO_4^{2-} and the extra -NH_2 effectively diluted the relative contribution of copper to the overall mass of Cu-AMTD.

As presented in Figure 2B, S2p XPS analysis clearly demonstrated the substantial presence of SO_4^{2-} within the Cu-AMTD. In stark contrast, the signal corresponding to SO_4^{2-} was negligibly detected in the spectrum of Cu-MTD, indicating a significantly lower level of SO_4^{2-} incorporation in the latter. This difference in sulfate incorporation was directly linked to the unique structural feature of the AMTD ligand – the presence of an accessible -NH_2, which was absent in the MTD ligand. Recent investigations in the field of Cu-azole materials synthesized from $CuSO_4$ had revealed that azole-based ligands containing -NH_2 group readily facilitated the co-incorporation of SO_4^{2-} into the resulting complexes. This phenomenon was driven by strong hydrogen bonding interactions formed between -NH_2 and SO_4^{2-} (ref: Small 2024, 2403850; Chem. Sci. 2024, 15, 19513).

Consequently, in the synthesis of Cu-AMTD from $CuSO_4$, the presence of the -NH_2 group in AMTD promoted the significant co-incorporation of SO_4^{2-} into the final complex structure. From a compositional perspective, the incorporated SO_4^{2-} (molar mass ≈ 96.06 g/mol), alongside the extra -NH_2 group within the AMTD ligand itself compared to MTD, constituted a considerable non-metallic mass fraction within the Cu-AMTD sample. Therefore, the substantial mass contribution from the incorporated SO_4^{2-} and the extra -NH_2 effectively diluted the relative contribution of copper to the overall mass of Cu-AMTD. This inherently led to a lower observed copper content compared to Cu-MTD. In contrast, Cu-MTD lacked -the extra NH_2 and SO_4^{2-}, thus leading to a higher content of Cu compared to Cu-AMTD.

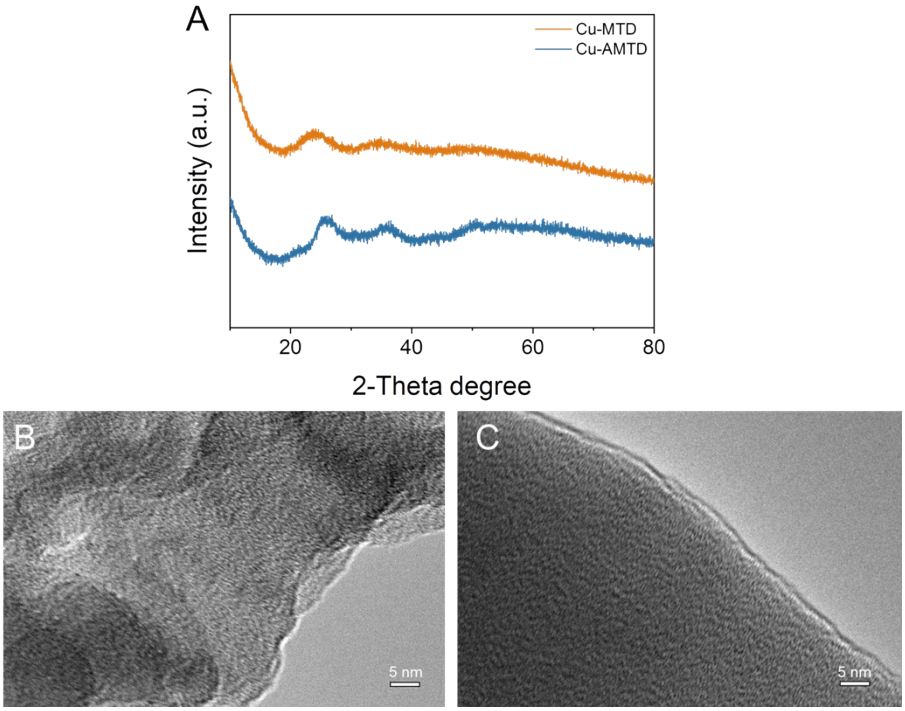

Figure S5 XRD patterns (A) and HRTEM images of Cu-AMTD (B) and Cu-MTD (C).

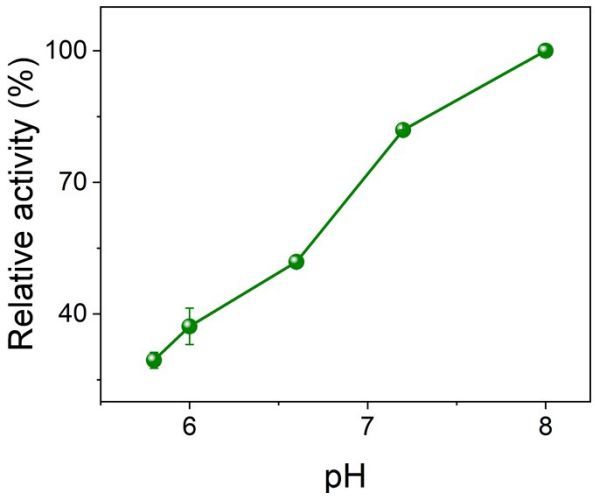

Figure S6 Catalytic activity of Cu-AMTD under different pHs.

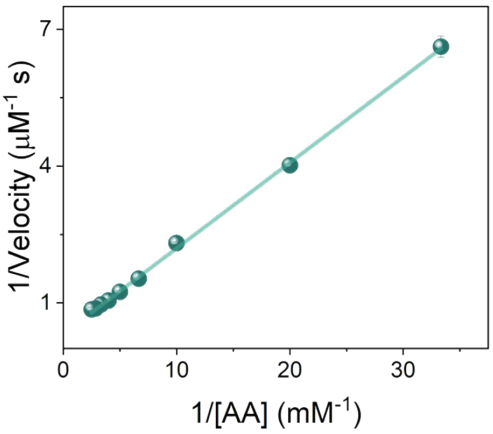

Figure S7 Lineweaver–Burk plot of Cu-AMTD.

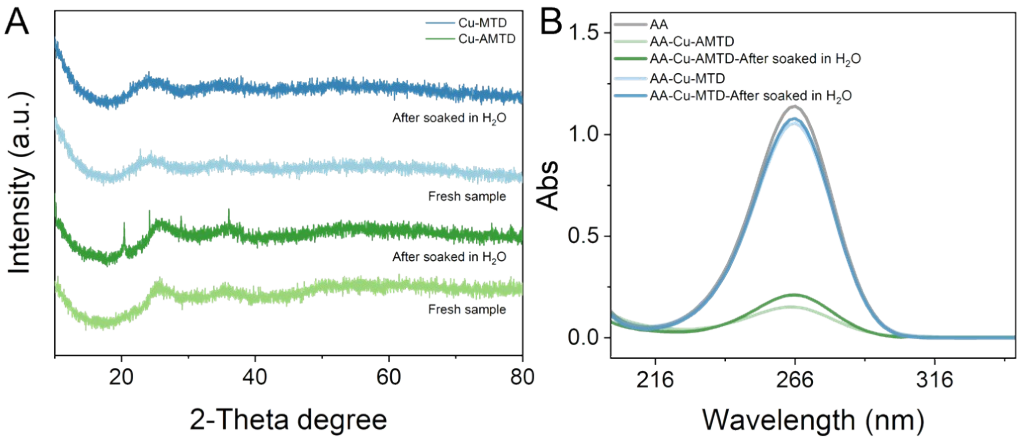

Figure S8 (A) XRD patterns of Cu-AMTD and Cu-MTD before and after soaked in H_2O; (B) UV−vis spectra of AA catalyzed by pristine and soaked Cu-AMTD and Cu-MTD in the PBS solution.

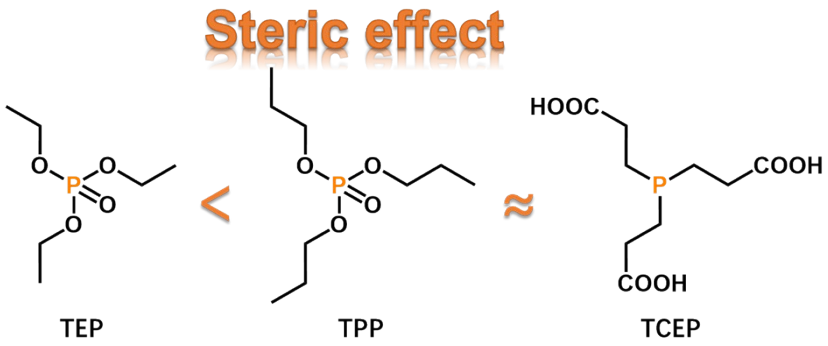

Figure S9 Molecular structures and steric effect of TEP, TPP and TCEP.

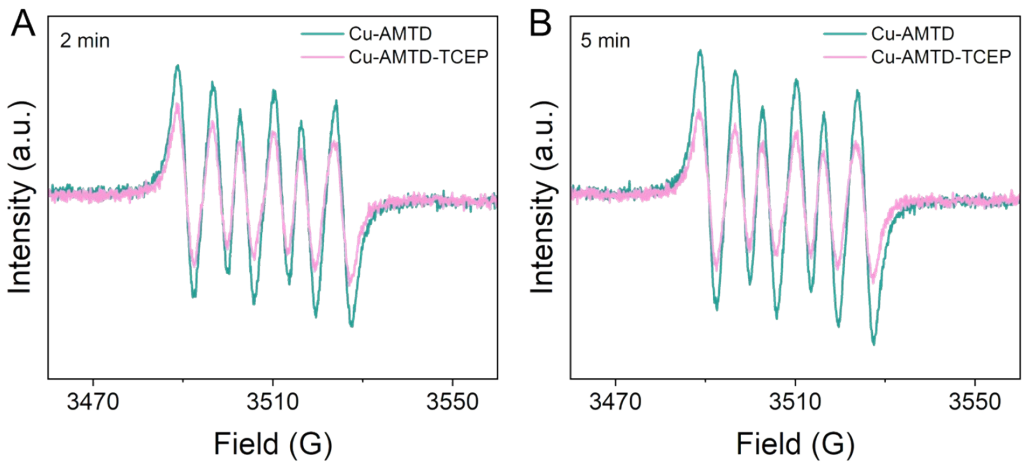

Figure S10 EPR-trapped $O_2^{\bullet-}$ signals of Cu-AMTD in the presence and absence of TCEP at 2 min (A) and 5 min (B).

TableS1 EXAFS data fitting parameters at the Cu *K*-edge for Cu-AMTD, Cu-MTD and Cu foil.

Sample	Path	*CN*[a]	*R*(Å)[b]	σ^2 (Å^2)[c]	ΔE_0(eV)[d]	*R* factor
Cu K-edge (S_0^2=0.809)						
Cu foil	Cu-Cu	12.0*	2.54±0.004	0.008	4.24±0.63	0.0033
Cu-AMTD	Cu-N	3.46±0.17	1.99±0.004	0.010	3.08	0.0070
	Cu-S	0.72±0.06	2.34±0.007	0.003	10.0	
Cu-MTD	Cu-N	3.33±0.37	2.03±0.03	0.012	3.8	0.009
	Cu-S	1.37±0.17	2.33±0.009	0.008	10.0	

[a]*CN*, coordination number; [b]*R*, the distance between absorber and backscatter atoms; [c]σ^2, the Debye Waller factor value; [d]ΔE_0, inner potential correction to account for the difference in the inner potential between the sample and the reference compound; *R* factor indicates the goodness of the fit. $S0^2$ was fixed to 0.809, according to the experimental EXAFS fit of Cu foil by fixing *CN* as the known crystallographic value. * This value was fixed during EXAFS fitting, based on the known structure of Cu. Fitting conditions: *k* range：3.0 - 12.0; *R* range: 1.0-3.0; fitting space: R space; *k*-weight = 3. A reasonable range of EXAFS fitting parameters: 0.700 < S_0^2 < 1.000; *CN* > 0; σ^2 > 0 Å^2; $|\Delta E_0|$ < 10 eV; *R* factor < 0.02.

Table S2 Comparison of AA oxidase-like activities between Cu-AMTD and other reported artificial enzymes and nanozymes.

Species	K_m(mM)	K_{cat} (s^{-1})	V_{max} ($\mu M\ s^{-1}$)	Buffer solution (ml)	Catalyst dosage (mg)	Ref.
CC-PtNPs	0.201	/	0.777	3.45	97.9	5
Ch-PtNPs	0.385	/	0.528	/	/	5
CS-PtNPs	0.404	/	1.447	3.4	54.8	6
b-Fe-GQDs	0.205	/	0.111	0.38	10	7
OPA-CsPbBr3	0.103	/	0.2303	0.9	1000	8
AgPd/C	0.6	/	0.0026	0.45	2.5	9
CuO NPs	0.1302	26.98	0.99	4	200	10
Fe-N-C	0.47	/	3.73	1	25	11
N-C	0.16	/	0.64	1	25	11
AA oxidase	0.07362	/	0.7334	0.48	5	this work
Cu-AMTD	0.5868	0.03026	3.12578	0.48	10	this work

Table S3 Comparison of various analysis methods for organophosphates detection.

Method	Catalyst	LOD (ppm)	Target analyte	Ref.
Colorimetric	AuNPs-CTAB	0.03	parathion	12
Fluorescence	$CuInS_2$ QDs	0.016	methyl parathion	13
Electrochemistry	ERGO-CS/Hb/FTO	0.021	methyl parathion	14
Colorimetric	AgNPs	11.29	chlorpyrifos	15
Optical	MPH	1.05	methyl parathion	16
Colorimetric	Aptamer-AuNPs	2.1×10^4	Omethoate	17
SERS	PDMS@Ag NPs	1	methyl parathion	18
SERS	AuNSs/PDMS	1.95	methyl parathion	19
HPLC-ELSD	H_2O_2	1.93	TCEP	20
Fluorescence	HC-N_3	0.023	TCEP	21
Chem-iluminescence	H_2O_2/Lucigenin	0.018	TCEP	22
Fluorescence	GNCs@BSA	0.032	TCEP	23
UV-Vis	Cu-AMTD	0.96	TCEP	this work

References

1 B. Jiang, D. Duan, L. Gao, M. Zhou, K. Fan, Y. Tang, J. Xi, Y. Bi, Z. Tong, G. F. Gao, N. Xie, A. Tang, G. Nie, M. Liang and X. Yan, *Nat. Protoc.*, 2018, **13**, 1506–1520.

2 F. He, L. Mi, Y. Shen, X. Chen, Y. Yang, H. Mei, S. Liu, T. Mori and Y. Zhang, *J. Mater. Chem. A*, 2017, **5**, 17413–17420.

3 Y. Hu, C.-Y. Li, X.-M. Wang, Y.-H. Yang and H.-L. Zhu, *Chem. Rev.*, 2014, **114**, 5572–5610.

4 A. V. Gurbanov, V. A. Aliyeva, R. M. Gomila, A. Frontera, K. T. Mahmudov and A. J. L. Pombeiro, *Cryst. Growth Des.*, 2023, **23**, 7335–7344.

5 S.-B. He, L. Yang, Y. Yang, H. A. A. Noreldeen, G.-W. Wu, H.-P. Peng, H.-H. Deng and W. Chen, *Carbohydr. Polym.*, 2022, **298**, 120120.

6 S.-B. He, L. Yang, M.-T. Lin, H. A. A. Noreldeen, R.-X. Yu, H.-P. Peng, H.-H. Deng and W. Chen, *Sens. Actuators B Chem.*, 2021, **347**, 130627.

7 H. Fan, W. Yang, Y. Dai, L. Huang, Q. Zhang, H. Zhang, J. Liu, W. Zhu and J. Hong, *Anal. Chim. Acta*, 2024, **1318**, 342931.

8 Q. Ye, E. Yuan, J. Shen, M. Ye, Q. Xu, X. Hu, Y. Shu and H. Pang, *Adv. Sci.*, 2023, **10**, 2304149.

9 L. Luo, J. Liu, Y. Liu, H. Chen, Y. Zhang, M. Liu and S. Yao, *Food Chem.*, 2024, **430**, 137062.

10 S. He, A. Hu, Q. Zhuang, H. Peng, H. Deng, W. Chen and G. Hong, *ChemBioChem*, 2020, **21**, 978–984.

11 X. Cao, C. Zhu, Q. Hong, X. Chen, K. Wang, Y. Shen, S. Liu and Y. Zhang, *Angew. Chem.*, 2023, **135**, e202302463.

12 S. Wu, D. Li, J. Wang, Y. Zhao, S. Dong and X. Wang, *Sens. Actuators B Chem.*, 2017, **238**, 427–433.

13 X. Yan, H. Li, Y. Yan and X. Su, *Food Chem.*, 2015, **173**, 179–184.

14 R. Kaur, S. Rana, K. Lalit, P. Singh and K. Kaur, *Biosens. Bioelectron.*, 2020, **167**, 112486.

15 P. Weerathunge, B. K. Behera, S. Zihara, M. Singh, S. N. Prasad, S. Hashmi, P. R. D. Mariathomas, V. Bansal and R. Ramanathan, *Anal. Chim. Acta*, 2019, **1083**, 157–165.

16 W. Lan, G. Chen, F. Cui, F. Tan, R. Liu and M. Yushupujiang, *Sensors*, 2012, **12**, 8477–8490.

17 P. Wang, Y. Wan, A. Ali, S. Deng, Y. Su, C. Fan and S. Yang, *Sci. China Chem.*, 2016, **59**, 237–242.

18 J. Sun, L. Gong, Y. Lu, D. Wang, Z. Gong and M. Fan, *Analyst*, 2018, **143**, 2689–2695.

19 X. Ma, J. Xie, Z. Wang and Y. Zhang, *Spectrochim. Acta. A. Mol. Biomol. Spectrosc.*, 2022, **267**, 120542.

20 Z. Tan, P. M. Ihnat, V. S. Nayak and R. J. Russell, *J. Pharm. Biomed. Anal.*, 2012, **59**, 167–172.

21 H. Guo, W. Tang and X. Duan, *Anal. Methods*, 2018, **10**, 5823–5826.

22 M. Saqib, S. Bashir, H. Li, S. Wang and Y. Jin, *Anal. Chem.*, 2019, **91**, 3070–3077.

23 T. Shu, J. Wang, L. Su and X. Zhang, *Anal. Chem.*, 2016, **88**, 11193–11198.